

SCIENTIFIC REPORTS



OPEN

Practical Three-Minute Synthesis of Acid-Coated Fluorescent Carbon Dots with Tuneable Core Structure

Stephen A. Hill¹, David Benito-Alifonso¹, Sean A. Davis¹, David J. Morgan², Monica Berry³ & M. Carmen Galan¹

We report a one-pot, three-minute synthesis of carboxylic acid-decorated fluorescent carbon dots (COOH-FCDs) with tuneable core morphology dependent on the surface passivating agent. Mechanism investigations highlighted the presence of key pyrazine and polyhydroxyl aromatic motifs, which are formed from the degradation of glucosamine in the presence of a bifunctional linker bearing acid and amine groups. The novel COOH-FCDs are selective Fe³⁺ and hemin sensors. Furthermore, the FCDs are shown to be non-toxic, fluorescent bioimaging agents for cancer cells.

In the last decade, nanotechnology has had a considerable impact on many research applications^{1–3}. An important focus area has been the development of fluorescent, non-toxic nanomaterials that can be tracked *in vivo* and *in vitro*^{4–8}, where fluorescent carbon dots (FCDs) provide an alternative to heavy metal-containing nanomaterials (e.g. quantum dots), due to their chemical inertness, high water solubility and very low cytotoxicity^{9–16}. These photoluminescent carbon-based materials have found applications in for example gene delivery^{9,17–19}, cell imaging¹², metal sensing^{11,20–22}, photo-catalysis²³ and photovoltaics^{23–26}. Due to their complex molecular structure, there is still a lack of fundamental understanding at the molecular level of their photoluminescence (PL) and chemical formation mechanisms, which has hampered the design of materials for specific applications²⁷. Understanding the formation mechanism and interdependence between core and surface features has been the focus of this study.

Although some microwave-assisted FCD syntheses are reported for a range of starting materials^{28–32}. Most reported FCDs syntheses require relatively harsh conditions (chemical or hydrothermal oxidation, pyrolysis, high acidic environments and long reactions times), elaborate post-modifications to improve the surface state of the nanomaterials and lengthy purifications^{12,33–35}, which makes the protocols difficult to handle by non-chemists at the point of use. Stemming from our interest in the development of facile protocols for the synthesis of fluorescent probes for biological applications^{36–40}, we turned our attention to the preparation of water soluble FCDs from commercial starting materials that are ready for conjugation by a given biomolecule. Herein, we report the practical one-pot three-minute synthesis of carboxylic acid-functionalised FCDs (COOH-FCD) from a carbohydrate starting material and an amino acid (Fig. 1). Following full physical and chemical characterisation, we show that the FCD core structure is highly dependent on the surface passivating agent chosen, reflecting events in the formation of these FCDs. Moreover, low toxicity exhibited by the novel nanomaterials highlights potential applications in environmental sensing and as cellular imaging probes.

Methods

Materials and Characterisation Methods. Chemicals were purchased and used without further purification. COOH-FCD formation was conducted in a domestic microwave oven (Tesco Microwave Oven MM07, Input Power: 1200 W, Microwave Output: 700 W). Concentration centrifugation tubes were GE Healthcare Life Sciences VIVASPIN 6/20 with a 10,000 Da molecular-weight cut off filter. Extracts were concentrated under reduced pressure using both a Büchi rotary evaporator at a pressure of either 15 mmHg (diaphragm pump) and 0.1 mmHg (oil pump), as appropriate, and a high vacuum line at room temperature. ¹H & ¹³C (HSQC and HMBC) NMR spectra were measured in D₂O on 500 MHz Varian. ¹H & ¹³C NMR chemical shifts are quoted in parts per million (ppm) and referenced to the residual solvent peak (D₂O: ¹H = 4.79 ppm); and coupling constants (J) given in Hertz. Multiplicities are abbreviated as: br (broad), s (singlet), d (doublet), t (triplet), q (quartet), p (pentet)

¹School of Chemistry, University of Bristol, Cantock's Close, Bristol, BS8 1TS, UK. ²Cardiff Catalysis Institute, School of Chemistry, Cardiff University, Park Place, Cardiff, CF10 3AT, UK. ³School of Physics, University of Bristol, Bristol, BS8 1TL, UK. Correspondence and requests for materials should be addressed to M.C.G. (email: m.c.galan@bristol.ac.uk)

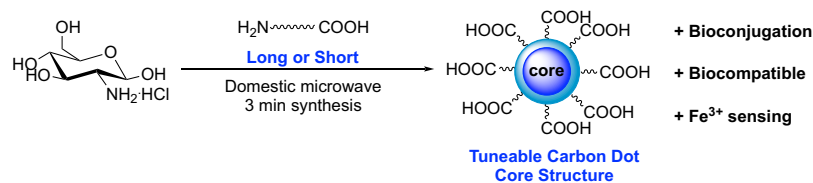


Figure 1. One-pot synthesis of carboxylic acid-coated carbon dots.

and m (multiplet) or combinations thereof. Assignments were made, where necessary, with the aid of HSQC and HMBC NMR experiments. Kochetkov's amination of unprotected carbohydrates was conducted using Biotage Initiator + microwave reactor. Fourier-transformed infra-red (FTIR) spectroscopy was conducted on a Bruker ATR. Dynamic Light Scattering (DLS) and Zeta analysis were carried out using Malvern Instruments, Nano-S90 Red Laser Model ZEN1690 for DLS and Nano-Z ZEN 2600 for Zeta potential. Zeta potential measurements were conducted in distilled H₂O. The structure of CDs were examined by transmission electron microscopy (TEM) on a Jeol 2100F with an accelerating voltage of 200 kV. A drop of the COOH-FCD methanol/water (1:2) suspension (5 mg/mL) was carefully applied to a 200-mesh carbon-coated copper grid and dried at ambient temperature for TEM characterization. TEM images were recorded using a Gatan SC1000 CCD camera and Gatan Microscopy Suite 3 (GMS 3) software. High resolution images were analyzed with GMS 3 to determine lattice spacings and ImageJ for particle sizing. Fluorescence measurements were made and conducted on a Perkin-Elmer LS45 in either 700 or 3500 μL quartz cuvettes (ThorLabs). Absorbance measurements were conducted on Cary UV-Vis 50 spectrophotometer in either 700 or 3500 μL quartz cuvettes (ThorLabs). Quantum yield of fluorescence (QY) measurements were conducted on both Perkin-Elmer LS45 and Cary UV-Vis 50 spectrophotometer in either 700 or 3500 μL quartz cuvettes (ThorLabs), relative to quinine sulfate (in 0.1 M H₂SO₄). X-ray photoelectron spectroscopy (XPS) was performed using a Kratos Axis Ultra DLD spectrometer, using monochromatic Al K α radiation operating at 144 W power (12 mA x 12 kV). For analysis, samples (dissolved in methanol/water (1:2)) were pipetted on to clean gold wafers and the solvent evaporated under vacuum in the fast-entry lock of the spectrometer. Analysis of all regions was taken at a pass energy of 20 eV with a 0.1 eV step for high resolution scans, and 150 eV and a 1 eV step for survey spectra. All data was subsequent calibrated to the lowest C(1s) line at 285 eV and quantified using sensitivity factors supplied by the manufacturer in CasaXPS v2.3.17PR1.1.

Synthetic Procedures. *Synthesis of 1-amino-15-oxo-4,7,10-trioxa-14-azaoctadecan-18-oic acid (TTA, 2).* To a solution of 4,7,10-trioxa-1,13-tridecanediamine (TTDDA) (1.00 g, 4.54 mmol) in MeCN (50 mL) was added portion-wise succinic anhydride (0.454 g, 4.54 mmol) with a high rate of stirring. The solution was left stirring for 17 h at room temperature. An oil-like precipitate was formed found underneath the bulk solvent. The residual MeCN was decanted and the resultant residue was reduced *in vacuo* to afford the mono acid 2 (1.39 g, 4.43 mmol) in a 95% yield. ¹H Presat NMR (500 MHz, D₂O) δ : 3.61–3.45 (10H, d, e), 3.43 (2H, t, J = 10 Hz, c), 3.12 (2H, t, J = 10 Hz, g), 2.98 (2H, t, J = 10 Hz, a), 2.50 (2H, t, J = 10 Hz, j), 2.38 (2H, t, J = 10 Hz, h), 1.79 (2H, p, J = 5 Hz, b), 1.65 (2H, p, J = 5 Hz, i); ¹³C NMR (125 MHz, D₂O) δ : 26, 28, 32, 33, 36, 37, 68, 69, 70, 71, 174, 175 ppm MS-ESI for C₁₄H₂₈N₂O₆ calc: 320.19; found: 343.20 [M + Na⁺].

Synthesis of COOH-FCD (4 and 5). To a stirring solution of glucosamine hydrochloride (1.00 g, 4.63 mmol) in distilled H₂O (20 mL) in a 250 mL conical flask, 1-amino-15-oxo-4,7,10-trioxa-14-azaoctadecan-18-oic acid 2 (1.64 g, 5.09 mmol, for 4) or β -alanine 3 (0.45 g, 5.09 mmol, for 5) was added and stirred to ensure homogeneity. The conical flask (without the stirring bar) was then placed in a domestic microwave (in a fume cupboard) and the solution heated for 3 mins at 700 Watts (full power). A viscous brown residue was afforded, which was dissolved in distilled H₂O (10 mL) and centrifuge-filtered through a GE Healthcare Life Sciences Vivaspin 20 MWCO 10000 spin column (8500 rpm, 30 mins). The filtrate was then reduced *in vacuo* (or lyophilised) to yield a thick brown oil, COOH-FCDs 4 or 5 (1–1.5 g).

Microwave-assisted Kochetkov's Amination of Lactose. The microwave vial was charged with unprotected lactose (0.25 g), ammonium carbonate (5-fold excess w/w over lactose, 1.25 g) and anhydrous DMSO (0.8 mL). The mixture was purged with N₂ and the tube was sealed and placed in an automated microwave at 600 C, 250 psi pressure and 10 watts power for 90 minutes. The reaction mixture was freeze dried overnight to remove excess ammonium carbonate and DMSO to afford β -glycosyl amines as hygroscopic solids. (1-aminolactose is typically a white or orange solid post-freeze drying). Conversion to aminoglycoside confirmed by Ninhydrin treatment.

Glyco-Functionalisation of COOH-FCD (6 and 7). To COOH-FCDs 4 or 5 (10 mg) in distilled H₂O (1 mL) was added CDI (1,1-carbonyldiimidazole, 40 mg) and the solution was sonicated for 15 min. Glycosylamine (lactose) 2 mL (10 mg mL⁻¹ solution) was added to the solution and this was stirred for 17 h in the dark. The reaction mixture was dialysed against distilled H₂O (500 MWCO) for 24 h (H₂O changed regularly). The resulting solution was reduced *in vacuo* to yield a brown product, 6 or 7 (10–15 mg).

Cell cultures, toxicity assays and confocal microscopy. *Cell culture.* MDA-MB-231 human breast cancer cells were grown in DMEM with 4.5 g glucose/L, GlutaMAX™ and 10% fetal bovine serum (FBS), and antibiotic-antimycotic solution (AntiAnti). Confluent cultures were dissociated using trypsin (Tryp LE Express) and plated at 10⁴ cells/well in either petri dishes (Mat-Tek 35 mm, with 14 mm glass microwell) for imaging,

or 96-well plates for toxicity tests. All cell culture media and additives were purchased from Invitrogen, Life Technologies (Thermo-Fisher).

Toxicity assays. All tests were conducted with 8 replicates per condition, i.e. toxicant concentration and time point, after exposures of 1 h, 1 day, and 3 days. Experiments were repeated at least twice. FCDs were applied at final concentrations from 2000 to 10^{-3} $\mu\text{g mL}^{-1}$ in medium with reduced FBS (5%), to allow cell division but avoid protection from high serum. The effects of **4** and **5** COOH-FCD on cell metabolism and viability were assessed using AlamarBlue and Calcein AM. AlamarBlue is cytosolic substrate (resazurin to resorufin) whose fluorescence spectrum changes on reduction. The number of live cells was evaluated using Calcein AM, which is enzymatically transformed into the fluorescent product Calcein in the cytoplasm of live cells. After exposure, cultures were washed with PBS, and incubated with both dyes simultaneously for 1 h. Fluorescence was measured on a CLARIOStar Microplate Reader at room temperature. Data are presented compared to control, unexposed cultures, on the same plate. Statistical analysis showed there was a significant interaction, between the concentration of either COOH-FCDs and the duration of exposure ($p < 0.0001$, Two Way ANOVA). The reductive metabolism per cell was significantly different for exposures of 1 h and 1 day, and 1 h and 3 days for either COOH-FCD ($p < 0.001$, corrected for multiple comparisons, respectively).

Confocal Microscopy. All images were acquired on a Leica SP5 confocal system equipped with a Leica DMI 6000 inverted microscope. For the excitation of the FCDs 405 nm excitation was used. Cells were live and imaged in Living Cell Imaging Solution (ThermoFisher Scientific). The images were analysed using Volocity software (PerkinElmer).

Results and Discussions

Synthesis of Acid functionalised FCDs. $\text{GlcNH}_2\cdot\text{HCl}$ **1** was chosen as the C source as it already contains a N required for heteroatom doping. This is an important and widely used strategy for improving the QY of CDs, since the introduction of N-doping allows the injection of electrons into the CD structure, which allows for new PL and fluorescence properties to be established²⁷. We hypothesised that the incorporation of a linker containing both a carboxylic acid and amine functionalities for surface passivation, would yield FCDs displaying surface acid groups, while maintaining PL properties. To that end, two different linkers bearing an amine and an acid group at each end, which differ in length and atomic nature, were chosen: 1-amino-15-oxo-4,7,10-trioxo-14-azaocadecan-18-oic acid⁴¹ (TTA, long linker) **2**, which was prepared on a gram-scale after reaction of TTDDA with succinic anhydride in MeCN in 95% yield and commercial β -alanine **3** (short-linker). Successful gram-scale, microwave-assisted (domestic 700 W MW) synthesis of COOH-FCDs was carried out using $\text{GlcNH}_2\cdot\text{HCl}$ **1** (1 equiv.) and either linker **2** or **3** (1.1 equiv.) in distilled water for 3 min. The reaction vessel is positioned always on the same spot on the MW plate to ensure batch-to batch reproducibility. Following dissolution in water and centrifugal filtration (10 kDa molecular weight cut-off) blue-fluorescent COOH-FCDs **4** and **5** were obtained (Figs 2 and S1 in ESI). To demonstrate the presence and accessibility of the surface-confined carboxylic acid groups, amide conjugation of **4** and **5** with 1-aminolactose using 1,1-carbonyldiimidazole (CDI) was performed and lactose-functionalised FCDs **6** and **7** were thus synthesised, as confirmed by ¹H-NMR after dialysis purification (Fig. 2 and Figs S25 and S26 in ESI).

Physical and Photoluminescence Characterisation. High-resolution transmission electron microscopy (HR-TEM) showed differences between the two COOH-FCDs systems, with TTA-decorated **4** having an average diameter (and standard deviation) of $2.78 \text{ nm} \pm 0.42$ (Fig. 3A,B) and $2.46 \text{ nm} \pm 0.44$ for β -alanine-decorated **5**. The increase in core diameter in COOH-FCD **4** is attributed to increased linker incorporation within the nanoparticle. Dynamic light scattering (DLS) indicated a hydrodynamic diameter of approximately 2–6 nm for COOH-FCDs **4** and 5–10 nm for **5** which we attributed to differences in solvation of the two nanoparticles (Fig. S2A,B in ESI). Both samples exhibited lattice fringes (Fig. S3A,B in ESI) which could be assigned to a graphitic structure^{42,43} and is in agreement with previously reported carbohydrate-derived FCDs^{43,44}. In both samples, spacings of 0.21 nm were most frequently observed corresponding to the (100) planes. Additional lattice fringes with interplanar spacings of 0.18 nm and 0.25 nm, which are assigned to graphitic (102) and (020) planes respectively, were scarcer. It is important to highlight that the diagnostic graphitic basal planar (002) spacings of 0.31 nm were only observed in sample **5**. This indicates that under the reaction conditions used, the core morphology of **4** is less-ordered, with the long linker retarding graphitization.

The PL properties were also evaluated, and near-identical profiles were observed for **4** and **5**. The TTA-functionalised COOH-FCD **4** absorbance profile maxima were between 200–450 nm, which is characteristic for bottom-up synthesized FCDs. The defined peak at 270 nm can be attributed to π - π^* transition of aromatic/alkenyl C=C bonds or C=N bonds (Fig. S4 in ESI)⁴⁵. The fluorescence emission profile ($\lambda_{\text{ex}} = 300$ –400 nm) exhibits the signature features of N-doped FCDs: blue-centred, excitation-dependent emission (Fig. 3C for **4**, and Fig. S5 in ESI for **5**). In addition, COOH-FCD **4** exhibited an optimal QY of 6% (for COOH-FCD **5**, QY = 4%), relative to quinine sulfate (Fig. S6). The excitation spectrum ($\lambda_{\text{em}} = 420 \text{ nm}$) shows two peaks at 230 nm (π - π^* of aromatic/alkenyl C=C bonds)⁴⁶, and 340 nm (n - π^* transitions in C=O/C=N bonds, Figs 3C and S5)⁴⁷. No photobleaching was recorded for either **4** and **5** after 30 min of continuous irradiation in-solution ($\lambda_{\text{ex}} = 340 \text{ nm}$, $\lambda_{\text{em}} = 440 \text{ nm}$, Figs S7 and 8), whereas Rhodamine 6 G showed a 50% reduction over the same time-period. Stability was further examined by monitoring the emissive intensity at pH 0–14. 100% intensity was retained between pH 6–10, and >75% from pH 3–6 and 10–11 for both particles, see ESI for details. COOH-FCDs **4** and **5** were also exposed to increasing concentrations of NaCl in aqueous solution to test the effect of ionic strength

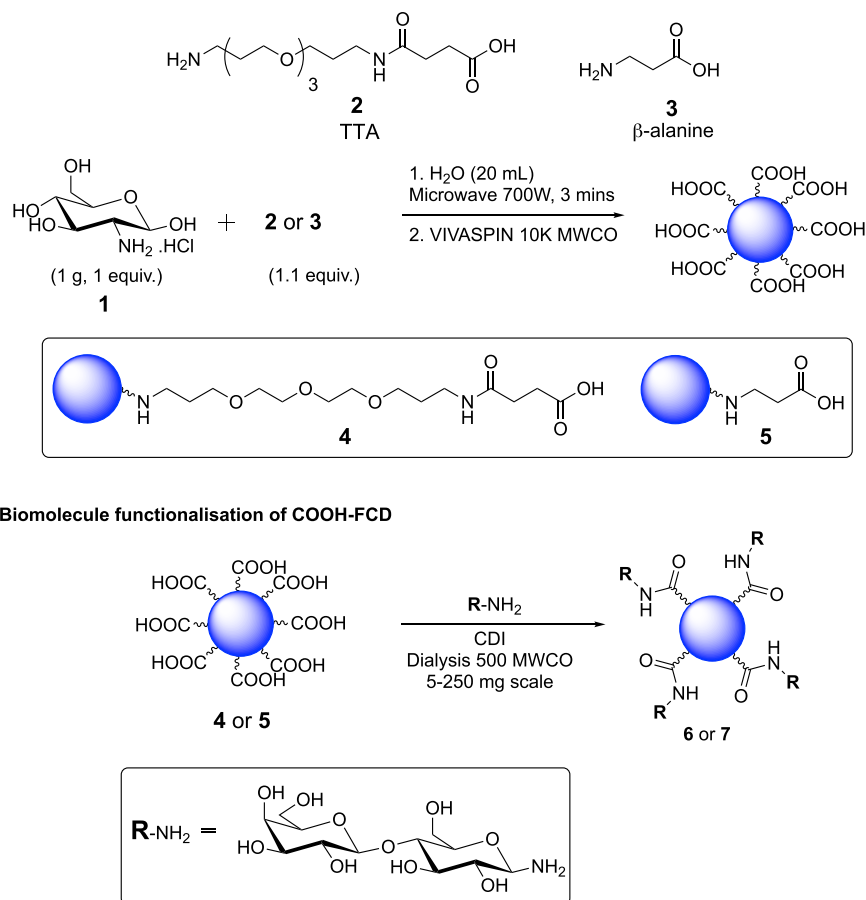


Figure 2. General synthetic preparation and lactose functionalization for COOH-FCDs **4** and **5**.

(Fig. S10). At salt concentrations of up to 1 M, a 13% reduction of emission was observed in both nanoparticles (see Fig. S10 in ESI), demonstrating the PL robustness of the newly synthesised COOH-FCDs.

The chemical and functional group composition of COOH-FCDs **4** and **5** was determined by elemental analysis, Fourier-transformed infra-red spectroscopy (FTIR) and x-ray photoelectron spectroscopy (XPS). As expected, differences in C and O composition between **4** and **5** were also detected in their elemental composition (For **4**, C: 38.04, H: 8.15, N: 6.37, Cl: 7.31, O: 40.11; and **5** was C: 47.27, H: 7.68, N: 7.69, Cl: 5.40, O: 31.95; Table S1), which is in agreement with the different nature of the passivating linkers, with TTA-derived COOH-FCD containing a greater proportion of O atoms in their structure than β -alanine. Functional group analysis by FTIR did not show significant differences between both COOH-FCDs (Figs S11 and 12). Signature peaks for COOH-FCD **4** were observed for amino and/or alcohol groups (N-H/O-H) at 3360 cm^{-1} . Signals at 2929 cm^{-1} , C-H (sp^3), were attributed to either the linker or to functional groups at the FCD surface. Amide groups (NHCO) at 1633 cm^{-1} indicated surface passivation, while a band centred at 1084 cm^{-1} could be assigned to C-O bonds of either the linker or residual carbohydrate. A large broad peak at 626 cm^{-1} indicated C-Cl bonds. A similar pattern was detected for **5**, see ESI Figs S11 and 12. XPS analyses gave near-identical results for both COOH-FCDs: the wide scan XPS spectrum for COOH-FCDs indicated the presence of C, O, N and Cl, in proportions similar to elemental analysis, with peaks at 285 eV (C 1s), 532 eV (O 1s), 400 eV (N 1s) and 197 eV (Cl 2p) for **4** (for **5** see Figs S13–16 ESI). High resolution scans of each peak were deconvoluted for functional group identification, and confirm the formation of aromatic C=O, -OH, and N-heteroaromatic moieties, as well as aliphatic C=O and C-Cl bonds (Tables S2 and 3).

The zeta potentials (electrokinetic potential) for COOH-FCDs **4** and **5** were in the range of -6.91 to $+3.01\text{ mV}$ for **4**, and -6.73 to $+2.29\text{ mV}$ for **5** (Figs S17 and 18). The values obtained in both cases are slightly more negative than previously produced FCD derived from diamine TTDA³⁹, which can be attributed to an increase of carboxylic acids on the surface. This is further supported by the increase of lactose functionalization (between 7–10 times) found on lactose-functionalised FCDs **6** and **7** when compared to TTDA-derived lactose FCDs³⁹ as determined by $^1\text{H-NMR}$ qualitative analysis of the ratio between one of the lactose anomeric signals ($\delta 4.57\text{ ppm}$) and a proton shift assigned to the FCD core at $\delta 5.07\text{ ppm}$ (see Fig. S27 and Table S4 in ESI), which suggests more acid groups are available for conjugation by the glycan biomolecule. Furthermore, these results also indicate a complex composition of surface functional groups, irrespective of linker length. Both COOH-FCD solubilities in aqueous media were excellent up to 20 mg mL^{-1} . Solutions exposed to light at room temperature for several months were stable. Structural characterization by NMR (Figs S19 and 20) revealed specific signals associated with the surface linkers: in the $^1\text{H NMR}$ of **4**, proton signals at $\delta 1.65, 1.83, 2.50, 2.98, 3.12, 3.43$ and

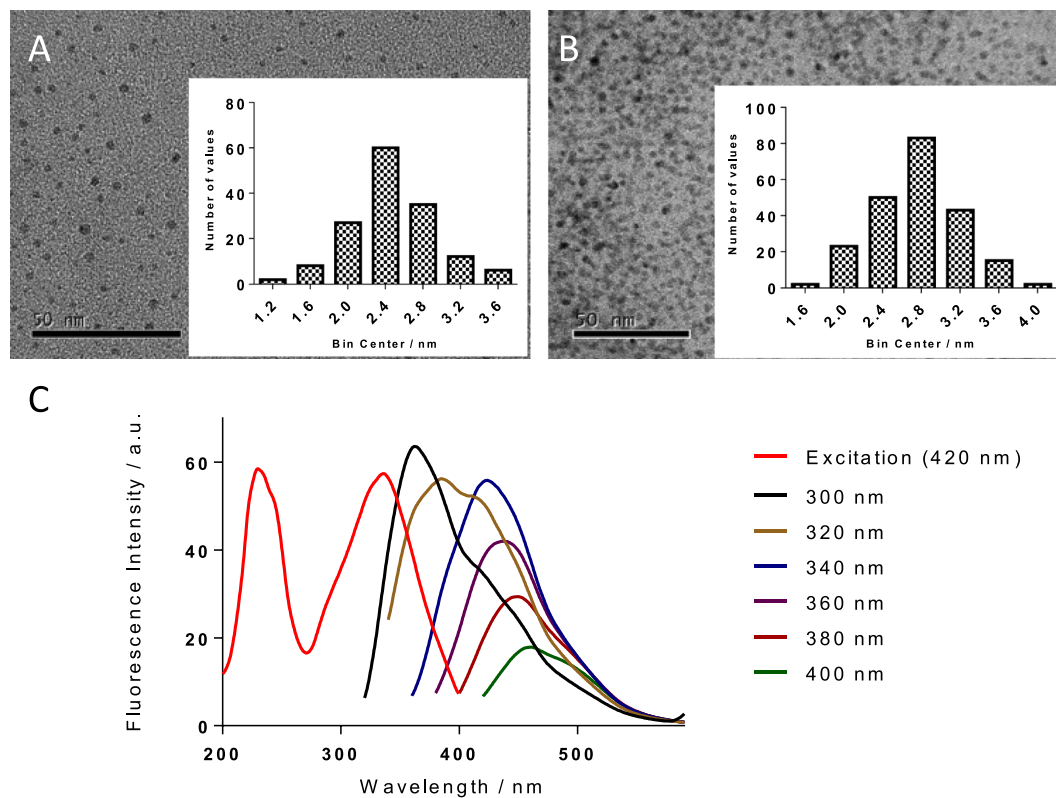


Figure 3. TEM images and sizing of (A) FCD 5 and (B) FCD 4 (number of values = number of particles); (C) excitation and emission spectrum of 4.

3.45–3.61 ppm; in **5** proton signals at δ 2.65 and 3.15 ppm associated to the β -alanine short linker. The presence of carboxylic acid surface functionality was further evidenced by the asymmetric nature of the conjugated linker highlighted in the $^1\text{H-NMR}$ - e.g. for **5**, the signature triplet splitting pattern assigned to the two central methylene groups in the β -alanine linker at δ 2.65 and 3.15 ppm, suggesting two different functional groups at either end (e.g. amide and acid groups) (Figs S19 and 20). In addition, two similar sets of signals with different intensity levels, suggested the presence of various organic species with lower intensity proton shifts between δ 2.50–4.50 ppm being assigned to surface-bound polyhydroxylated architectures. $^1\text{H-}^{13}\text{C}$ HMBC NMR analysis of these peaks revealed correlations with cross-peaks at 170–185 ppm signifying closely connected amorphous/ sp^3 and sp^2 -surface domains (Figs S21 and 22). ^1H NMR, identified conserved and well-resolved singlets at σ 8.38, 8.56 and 5.00 ppm in both COOH-FCD **4** and **5**. $^1\text{H-}^{13}\text{C}$ HSQC and HMBC NMR experiments further uncovered the likely molecular structure of these conserved signals, (Figs S21 and 24). One-bond correlations between proton shifts at δ 5.00 ppm and ^{13}C signals at 70 ppm and 2–3 bond connectivity to aromatic carbon shifts at σ 142 and 154 ppm were also unveiled, which can be assigned to pyrazine motifs. Moreover, singlets at δ 8.38 and 8.56 ppm, associated to *N*-heteroaromatic species⁴⁷, showed direct connectivity to aromatic carbon signals at 144 and 142 ppm, respectively, and 2–3 bond correlations to a signal at 154 ppm. These results indicate the presence of simple *N*-heteroaromatic species, likely a pyrazine-type motif⁴⁸. 1,2-aminoaldoses, which we have identified as a key intermediate in the synthesis of FCDs from glucosamine³⁹, can self-dimerise in a sequential cyclisation/condensation reaction to afford pyrazine rings with polyhydroxyl arms derived from the remaining carbohydrate moiety^{49–52}. Indeed, the formation of fructosazine, a polyhydroxylpyrazine from the browning of glucosamine is a well-studied reaction⁵³. Thus, we suspect a similar polyhydroxylpyrazine as a common motif in both COOH-FCDs **4** and **5**.

Mechanism of COOH-FCD Formation. In order to ascertain the reaction mechanism of the formation of COOH-FCDs, a time-point ^1H and ^{13}C NMR analysis of the reaction was carried out at 30 s intervals up to 180 s. β -alanine-derived FCD **5** was chosen as the model system, as both FCDs exhibit the same conserved signals in NMR spectra (Figs S28 and 29). Although pyrazine-type signals (δ 8.40 and 8.55 ppm) start appearing slowly at 30 s of MW heating, significant formation occurs only after 120 s. Carbohydrate anomeric signals δ 4.60–5.30 ppm, assigned to the ring-closed pyranose, also undergo significant change after 120 s. This transition, after 2 minutes of MW irradiation, is also evident in the ^{13}C NMR spectra: loss of the anomeric carbon at σ 90 ppm, increased complexity of aromatic-associated signals (σ 140–180 ppm) and variations in signals at δ 20–80 ppm; the latter assigned to the pyranose ring (Fig. S29). Moreover, after 120 s MW heating, the characteristic carbonyl $\text{C}=\text{O}$ signal from an acid functional group was observed in the ^{13}C spectra at δ 177 ppm signal, further confirming the presence of acid groups on the FCD surface. After the first 120 s, loss of solvent leads to a critical concentration of precursors, in which subsequent carbonisation and aromatisation can occur, leading to the formation

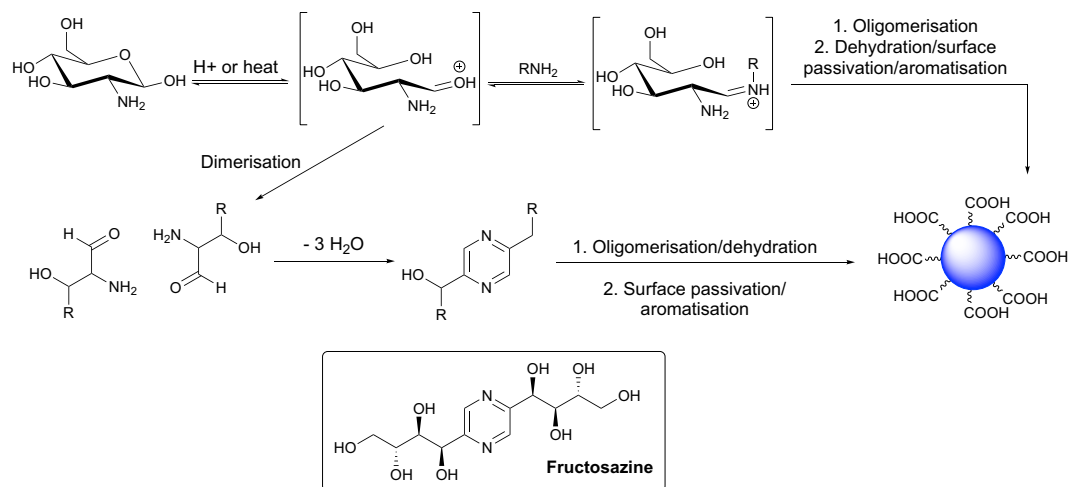


Figure 4. Proposed mechanism of COOH-FCD formation.

of the pyrazine-type motif (Fig. 4 and S1 in ESI). Interestingly, the PL properties of **5** measured at different reaction times (from 30 to 150 s) did not significantly change the emission profile with the exception emission at $\lambda_{\text{ex}} = 300$ nm, which was optimum at 120 s. These results suggest that fluorophores contributing to the PL properties of the material are generated early on in the synthesis with an optimum profile at 120 s (See Figure S30 in ESI).

Fe³⁺ Sensing Studies. The development of fast and cheap technologies to detect Fe³⁺ species is of great interest for monitoring water quality and for understanding biological processes^{54,55}. The redox properties of Fe³⁺ are part of important physiological processes⁵⁵. Qualitative and quantitative Fe³⁺ detection can be achieved by voltammetry^{56,57}, atomic absorption spectrometry⁵⁸, and inductively coupled plasma mass spectrometric (ICP-MS) methods⁵⁹. Most detection methods use emissive species such as organic dyes⁶⁰, QDs⁶¹, and metal-organic frameworks^{62–65}, which are quenched in the presence of Fe³⁺. However, these materials are often expensive and protocols to access them are labour-intensive. Moreover, most fluorophores are often not temperature, light or air-photostable. The use of water soluble FCDs as heavy metal sensors for Hg²⁺, Fe³⁺, Cr²⁺ has been described in recent years²⁰, although little is known about the sensing mechanisms.

In addition to pyrazine-type moieties, we also identified the presence of polyhydroxyl aromatics in the surface of COOH-FCDs **4** and **5**. We thus hypothesised that COOH-FCDs could act as selective sensors for Fe³⁺ in a similar fashion to catechol-siderophores: 1,2-hydroxybenzene motifs (catechols) can strongly chelate to Fe³⁺ due to a hard-hard interaction, as defined by Hard-Soft Acid-Base (HSAB) theory⁶⁶. For instance, enterobactin, a common siderophore in mainly Gram-negative bacteria, uses several catechol motifs to selectively scavenge Fe³⁺ over Fe²⁺⁶⁷. To explore this application, 500 μM solutions of metal chloride salts of Fe³⁺, Fe²⁺, Ca²⁺, Cu⁺, Cu²⁺, Mn²⁺, and Mg²⁺, in addition to a wide range of salts containing those metals, were exposed to FCD **4** in deionized (dd)-water (see Fig. S32 in ESI). While minimal fluorescence depletion was observed with all tested salts, significant quenching (around 91%) was observed for Fe³⁺. Fe²⁺ only quenched the FCD fluorescence by 15%, which implies siderophore-type selectivity. Next, the effect of linker length and atomic nature on COOH-FCDs **4** and **5** towards Fe³⁺ sensing was evaluated in a Fe³⁺ titration experiment (0–500 μM in dd-water, Fig. S33). Overall, a 10% decrease in fluorescent quenching was observed for COOH-FCD **4**, which bears a longer linker. This result highlights the requirement for interactions between the Fe³⁺ and the polyhydroxyl aromatics and sp² surface domains in the COOH-FCD. The steric bulk of the linker appears to interfere by somewhat blocking the surface emissive centres. To explore the selectivity for Fe³⁺ detection in a biologically relevant molecule, hemin, which contains a ferric cation surrounded by a protoporphyrin ligand, was examined. Hemin fluorescence quenching of **4** and **5** was superior to that for Fe³⁺ (Fig. 5). For example, at 10 μM , a 10% decrease was measured for Fe³⁺ and a 73% decrease in hemin emission was observed, 95% of the FCD fluorescence was quenched when COOH-FCDs **5** was exposed to 40 μM hemin. We attribute the enhanced quenching effect for hemin to the presence of the porphyrin motif, which allows for additional π - π stacking interactions to the COOH-FCD surface sp²-domains.

Acid coated-FCDs for live cell imaging. The biocompatibility of COOH-FCDs with cells is an absolute requirement for their use in live cell imaging applications. To that end, cell toxicity and internalisation studies were conducted in MDA-MB-231 (human breast) cancer cells. MDA cultures were exposed to concentrations from 10⁻³ to 2000 $\mu\text{g mL}^{-1}$ for 1 hour, 1 and 3 days. Reductive metabolic (RM) competence was assessed by Alamar Blue, and the number of live cells with Calcein AM. Neither long linker COOH-FCD **4** or β -alanine-derived COOH-FCD **5** caused significant cell death at any exposure, duration and concentrations tested (Figs S34 and S35). RM alterations were measured after 1 h exposure at all tested concentrations. RM decreased to 60% after 3 days of continuous exposure at 2000 $\mu\text{g mL}^{-1}$, highlighting interactions between FCD and cells. For either COOH-FCD LC₅₀ was not reached even at the highest concentration and longest exposure.

Confocal microscopy was used to monitor cellular uptake, evaluated as fluorescence per unit area (FPUA). In live MDA cells after 2 h exposure to 500 $\mu\text{g mL}^{-1}$ of both COOH-FCDs at 4 °C and 37 °C (Fig. 6), there were no

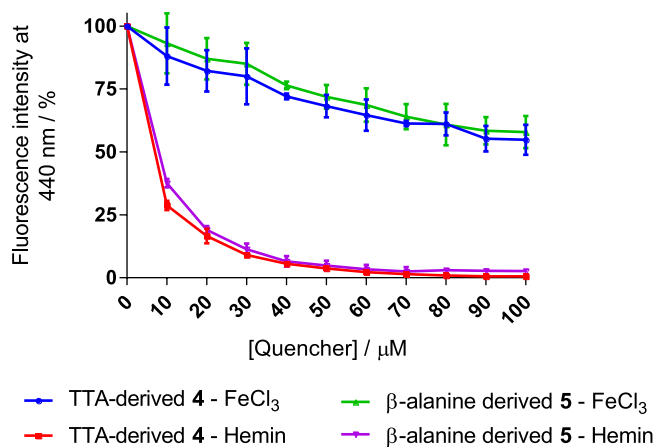


Figure 5. Comparison of quenching with Fe^{3+} and hemin of 4 and 5 in deionised water.

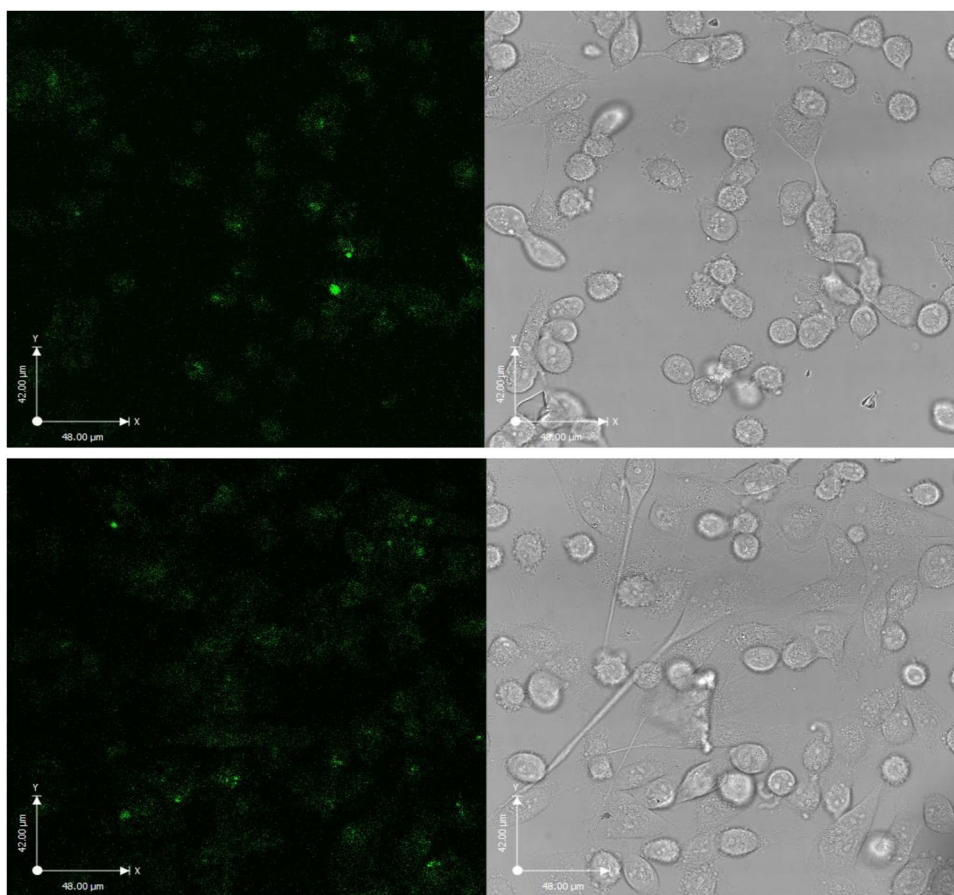


Figure 6. Confocal microscopy images of COOH-FCD 5 internalization in MDA cells exposed to $500 \mu\text{g mL}^{-1}$ for 2 h: (Top) 4°C and (Bottom) 37°C .

FPUA differences (Fig. S36), suggesting passive transport, without energy input, as internalization pathways for either FCD (for complete set of images including images of untreated cells see S37–39).

Conclusion

In summary, we have shown the one-pot three-minute synthesis of carboxylic-acid FCDs (COOH-FCDs) from cheap and easily-accessible starting materials. The different COOH-FCDs bear similar surface functional groups, structural and PL properties, while the core structure, however, depends on the passivating agent. β -alanine-derived FCDs (5) result in more crystalline graphitic (sp^2) cores, whereas TTA-linkers, which are longer and bear a higher O content, yield FCDs (4) with less ordered cores. We also show that the CDs are

stable in a range of pH from 3–11 without significant loss of fluorescence. Moreover, the CDs were stable to purification on silica gel column and size-exclusion chromatography (G10 Sephadex). Control over the core morphology, provides unique opportunities to probe PL mechanisms as well as the tribological properties of these novel materials. A key pyrazine-type motif, which is likely generated from the self-dimerisation of the 1,2-aminoaldose intermediate, leads to disubstituted polyhydroxyl pyrazine motifs, e.g. fructosazine. The latter, upon continued heating and dehydration leads to FCD formation. We show that the novel COOH-FCDs can selectively detect Fe³⁺ and hemin in deionised water, which further supports the presence of the identified surface functional groups. Finally, we demonstrate that COOH-FCDs are readily internalised in MDA-MB-231 cancer cells via a passive uptake pathway and that the FCDs are non-toxic at high concentrations and very long continuous exposures.

References

- Janib, S. M., Moses, A. S. & MacKay, J. A. Imaging and drug delivery using theranostic nanoparticles. *Adv. Drug Deliv. Rev.* **62**(11), 1052–1063 (2010).
- Xie, J., Lee, S. & Chen, X. Nanoparticle-based theranostic agents. *Adv. Drug Deliv. Rev.* **62**(11), 1064–1079 (2010).
- Hahn, M. A., Singh, A. K., Sharma, P., Brown, S. C. & Moudgil, B. M. Nanoparticles as contrast agents for *in-vivo* bioimaging: current status and future perspectives. *Anal. Bioanal. Chem.* **399**(1), 3–27 (2011).
- Tallury, P., Malhotra, A., Byrne, L. M. & Santra, S. Nanobioimaging and sensing of infectious diseases. *Adv. Drug Deliv. Rev.* **62**(4), 424–437 (2010).
- Xu, G. *et al.* New Generation Cadmium-Free Quantum Dots for Biophotonics and Nanomedicine. *Chem. Rev.* **116**(19), 12234–12327 (2016).
- Jin, Y. & Gao, X. Plasmonic fluorescent quantum dots. *Nat. Nano* **4**(9), 571–576 (2009).
- Wen, J., Xu, Y., Li, H., Lu, A. & Sun, S. Recent applications of carbon nanomaterials in fluorescence biosensing and bioimaging. *Chem. Commun.* **51**(57), 11346–11358 (2015).
- Geszke-Moritz, M. & Moritz, M. Quantum dots as versatile probes in medical sciences: Synthesis, modification and properties. *Mat. Sci. Eng. C* **33**(3), 1008–1021 (2013).
- Liu, W. *et al.* Carbon dots: surface engineering and applications. *J. Mat. Chem. B* **4**(35), 5772–5788 (2016).
- Li, H., Kang, Z., Liu, Y. & Lee, S.-T. Carbon nanodots: synthesis, properties and applications. *J. Mat. Chem.* **22**(46), 24230–24253 (2012).
- Lim, S. Y., Shen, W. & Gao, Z. Carbon quantum dots and their applications. *Chem. Soc. Rev.* **44**(1), 362–381 (2015).
- Baker, S. N. & Baker, G. A. Luminescent Carbon Nanodots: Emergent Nanolights. *Angew. Chem. Int. Ed.* **49**(38), 6726–6744 (2010).
- Xu, X. *et al.* Electrophoretic Analysis and Purification of Fluorescent Single-Walled Carbon Nanotube Fragments. *J. Am. Chem. Soc.* **126**(40), 12736–12737 (2004).
- Zhang, Q. G. *et al.* Graphene structure boosts electron transfer of dual-metal doped carbon dots in photooxidation. *Carbon* **126**, 128–134 (2018).
- Shao, X. D. *et al.* Engineering surface structure of petroleum-coke-derived carbon dots to enhance electron transfer for photooxidation. *J. Catal.* **344**, 236–241 (2016).
- Wu, W. *et al.* Synergies between Unsaturated Zn/Cu Doping Sites in Carbon Dots Provide New Pathways for Photocatalytic Oxidation. *ACS Catal.* **8**, 747–753 (2018).
- Hu, L. *et al.* Multifunctional carbon dots with high quantum yield for imaging and gene delivery. *Carbon* **67**, 508–513 (2014).
- Liu, C. *et al.* Nano-carrier for gene delivery and bioimaging based on carbon dots with PEI-passivation enhanced fluorescence. *Biomaterials* **33**(13), 3604–3613 (2012).
- Cheng, L. *et al.* Polycation-b-Polyzwitterion Copolymer Grafted Luminescent Carbon Dots As a Multifunctional Platform for Serum-Resistant Gene Delivery and Bioimaging. *ACS Appl. Mat. Interf.* **6**(22), 20487–20497 (2014).
- Gao, X., Du, C., Zhuang, Z. & Chen, W. Carbon quantum dot-based nanoprobe for metal ion detection. *J. Mat. Chem. C* **4**(29), 6927–6945 (2016).
- Roy, P., Chen, P.-C., Periasamy, A. P., Chen, Y.-N. & Chang, H.-T. Photoluminescent carbon nanodots: synthesis, physicochemical properties and analytical applications. *Mat. Today* **18**(8), 447–458 (2015).
- Dong, Y., Cai, J., You, X. & Chi, Y. Sensing applications of luminescent carbon based dots. *Analyst* **140**(22), 7468–7486 (2015).
- Hutton, G. A. M., Martindale, B. C. M. & Reisner, E. Carbon dots as photosensitisers for solar-driven catalysis. *Chem. Soc. Rev.* (2017).
- Li, X., Rui, M., Song, J., Shen, Z. & Zeng, H. Carbon and Graphene Quantum Dots for Optoelectronic and Energy Devices: A Review. *Advanced Functional Materials* **25**(31), 4929–4947 (2015).
- Shen, J., Zhu, Y., Yang, X. & Li, C. Graphene quantum dots: emergent nanolights for bioimaging, sensors, catalysis and photovoltaic devices. *Chem. Commun.* **48**(31), 3686–3699 (2012).
- Yan, X., Cui, X., Li, B. & Li, L.-S. Large, Solution-Processable Graphene Quantum Dots as Light Absorbers for Photovoltaics. *Nano Letters* **10**(5), 1869–1873 (2010).
- Hill, S. & Galan, M. C. Fluorescent carbon dots from mono- and polysaccharides: synthesis, properties and applications. *Beilst. J. Org. Chem.* **13**, 675–693 (2017).
- He, G. L. *et al.* Rapid solid-phase microwave synthesis of highly photoluminescent nitrogen-doped carbon dots for Fe³⁺ detection and cellular bioimaging. *Nanotechnology* **27**, 39 (2016).
- Xu, M. H. *et al.* Hydrophilic and blue fluorescent N-doped carbon dots from tartaric acid and various alkylol amines under microwave irradiation. *Nanoscale* **7**(38), 15915–15923 (2015).
- Wang, D. *et al.* Fluorescent carbon dots from milk by microwave cooking. *Rsc Adv* **6**(47), 41516–41521 (2016).
- Song, L., Cui, Y. Y., Zhang, C. F., Hu, Z. B. & Liu, X. F. Microwave-assisted facile synthesis of yellow fluorescent carbon dots from o-phenylenediamine for cell imaging and sensitive detection of Fe³⁺ and H₂O₂. *Rsc Adv* **6**(21), 17704–17712 (2016).
- Zhu, H. *et al.* Microwave synthesis of fluorescent carbon nanoparticles with electrochemiluminescence properties. *Chem Commun* **34**, 5118–5120 (2009).
- Dong, Y. *et al.* Carbon-Based Dots Co-doped with Nitrogen and Sulfur for High Quantum Yield and Excitation-Independent Emission. *Angew. Chem. Int. Ed.* **52**(30), 7800–7804 (2013).
- Song, Y. *et al.* Investigation from chemical structure to photoluminescent mechanism: a type of carbon dots from the pyrolysis of citric acid and an amine. *J. Mat. Chem. C* **3**(23), 5976–5984 (2015).
- Dong, Y. *et al.* Polyamine-functionalized carbon quantum dots for chemical sensing. *Carbon* **50**(8), 2810–2815 (2012).
- Benito-Alifonso, D. *et al.* Lactose as a “Trojan Horse” for Quantum Dot Cell Transport. *Angew. Chem. Int. Ed.* **53**, 810–814 (2014).
- Hou, B. *et al.* Initial stages in the formation of Cu₂ZnSn(S,Se)₄ nanoparticles. *Chem. Eur. J.* **19**, 15847–15851 (2013).
- Hou, B. *et al.* Rapid Phosphine-Free Synthesis of CdSe Quantum Dots: Promoting the Generation of Se Precursors by a Radical Initiator. *J. Mat. Chem. A* **2**, 6879–6886 (2014).

39. Hill, S. A. *et al.* Three-minute synthesis of sp³ nanocrystalline carbon dots as non-toxic fluorescent platforms for intracellular delivery. *Nanoscale* **8**(44), 18630–18634 (2016).
40. Miles, B. T. *et al.* Direct Evidence of Lack of Colocalisation of Fluorescently Labelled Gold Labels Used in Correlative Light Electron Microscopy. *Scientific Reports*. **7**, 44666 (2017).
41. Kim, M. *et al.* Antibody-free peptide substrate screening of serine/threonine kinase (protein kinase A) with a biotinylated detection probe. *Anal. Biochem.* **413**(1), 30–35 (2011).
42. Crystallography Open Database entry number 96-101-1081, graphite 2H.
43. Guo, X., Wang, C.-F., Yu, Z.-Y., Chen, L. & Chen, S. Facile access to versatile fluorescent carbon dots toward light-emitting diodes. *Chem. Commun.* **48**, 2692–2694 (2012).
44. Yang, Z.-C. *et al.* Intrinsically fluorescent carbon dots with tunable emission derived from hydrothermal treatment of glucose in the presence of monopotassium phosphate. *Chem. Commun.* **47**(42), 11615–11617 (2011).
45. Ding, H., Wei, J.-S. & Xiong, H.-M. Nitrogen and sulfur co-doped carbon dots with strong blue luminescence. *Nanoscale* **6**(22), 13817–13823 (2014).
46. Tan, J. *et al.* Large-scale synthesis of N-doped carbon quantum dots and their phosphorescence properties in a polyurethane matrix. *Nanoscale* **8**(8), 4742–4747 (2016).
47. Yuan, Y. H. *et al.* Synthesis of nitrogen-doping carbon dots with different photoluminescence properties by controlling the surface states. *Nanoscale* **8**(12), 6770–6776 (2016).
48. Sommer, H. *et al.* Determination of the substitution pattern of di- and trisubstituted pyrazines by 15N, 13C and 1H NMR spectroscopy. *Magn. Reson. Chem.* **38**, 907–917 (2000).
49. Klinger, K. M., Liebner, F., Fritz, I., Potthast, A. & Rosenau, T. Formation and Ecotoxicity of N-Heterocyclic Compounds on Ammoxidation of Mono- and Polysaccharides. *J. Agric. Food Chem.* **61**(38), 9004–9014 (2013).
50. Hwang, H.-I., Hartman, T. G., Rosen, R. T., Lech, J. & Ho, C.-T. Formation of Pyrazines from the Maillard Reaction of Glucose and Lysine- α -amine-15N. *J. Agric. Food Chem.* **42**(4), 1000–1004 (1994).
51. Shibamoto, T. & Bernhard, R. A. Investigation of Pyrazine Formation Pathways in Glucose-Ammonia Model Systems. *Agric. Biol. Chem.* **41**(1), 143–153 (1977).
52. Hrynets, Y., Ndagijimana, M. & Betti, M. Studies on the Formation of Maillard and Caramelization Products from Glucosamine Incubated at 37°C. *J. Agric. Food Chem.* **63**(27), 6249–6261 (2015).
53. Bhattacharjee, A., Hrynets, Y. & Betti, M. Fructosazine, a Polyhydroxyalkylpyrazine with Antimicrobial Activity: Mechanism of Inhibition against Extremely Heat Resistant Escherichia coli. *J. Agric. Food Chem.* **64**(45), 8530–8539 (2016).
54. Carter, K. P., Young, A. M. & Palmer, A. E. Fluorescent Sensors for Measuring Metal Ions in Living Systems. *Chem. Rev.* **114**(8), 4564–4601 (2014).
55. McRae, R., Bagchi, P., Sumalekshmy, S. & Fahrni, C. J. *In Situ* Imaging of Metals in Cells and Tissues. *Chem. Rev.* **109**(10), 4780–4827 (2009).
56. McBride, N. S. & Hall, E. A. H. Fe³⁺/Fe²⁺ Mycobactin-Complex Electrochemistry as an Approach to Determine Mycobactin Levels in Urine. *Electroanal.* **27**(3), 833–842 (2015).
57. Zamani, H. A. & Faridbod, F. Liquid membrane potentiometric sensor for determination of Fe³⁺ ion. *J. Anal. Chem.* **69**(11), 1073–1078 (2014).
58. Korn, Md. G. A. *et al.* Atomic spectrometric methods for the determination of metals and metalloids in automotive fuels – A review. *Talanta* **73**(1), 1–11 (2007).
59. Ferrarello, C., Fernández de la Campa, M. & Sanz-Medel, A. Multielement trace-element speciation in metal-biomolecules by chromatography coupled with ICP-MS. *Anal. Bioanal. Chem.* **373**(6), 412–421 (2002).
60. Lohani, C. R., Kim, J.-M. & Lee, K.-H. Facile synthesis of anthracene-appended amino acids as highly selective and sensitive fluorescent Fe³⁺ ion sensors. *Bioorg. Med. Chem. Lett.* **19**(21), 6069–6073 (2009).
61. Wu, P., Li, Y. & Yan, X.-P. CdTe Quantum Dots (QDs) Based Kinetic Discrimination of Fe²⁺ and Fe³⁺, and CdTe QDs-Fenton Hybrid System for Sensitive Photoluminescent Detection of Fe²⁺. *Anal. Chem.* **81**(15), 6252–6257 (2009).
62. Zheng, M. *et al.* Fast Response and High Sensitivity Europium Metal Organic Framework Fluorescent Probe with Chelating Terpyridine Sites for Fe³⁺. *ACS Appl. Mat. Interf.* **5**(3), 1078–1083 (2013).
63. Yang, C.-X., Ren, H.-B. & Yan, X.-P. Fluorescent Metal–Organic Framework MIL-53(Al) for Highly Selective and Sensitive Detection of Fe³⁺ in Aqueous Solution. *Anal. Chem.* **85**(15), 7441–7446 (2013).
64. Xu, H. *et al.* Metal-organic framework nanosheets for fast-response and highly sensitive luminescent sensing of Fe³⁺. *J. Mat. Chem. A* **4**(28), 10900–10905 (2016).
65. Cao, L.-H., Shi, F., Zhang, W.-M., Zang, S.-Q. & Mak, T. C. W. Selective Sensing of Fe³⁺ and Al³⁺ Ions and Detection of 2,4,6-Trinitrophenol by a Water-Stable Terbium-Based Metal–Organic Framework. *Chem. Eur. J.* **21**(44), 15705–15712 (2015).
66. Pearson, R. G. Hard and Soft Acids and Bases. *J. Am. Chem. Soc.* **85**(22), 3533–3539 (1963).
67. Hider, R. C. & Kong, X. Chemistry and biology of siderophores. *Nat. Prod. Rep.* **27**(5), 637–657 (2010).

Acknowledgements

This research was supported by EPSRC CAF EP/L001926/1 (MCG), ERC-COG: 648239 (MCG) and EPSRC EP/G036764/1 (SAH). Thanks to Dr. D. Alibhai (Wolfson Bioimaging Facility) for confocal assistance, and Mr. J. Jones for assistance with TEM (Chemistry Imaging Facility with equipment funded by UoB and EPSRC (EP/K035746/1 and EP/M028216/1)).

Author Contributions

S.A.H. and M.C.G. conceived the experiments, S.A.H. and D.B.A. conducted the synthesis and characterization of materials, S.A.D. carried out the TEM analysis, D.J.M. performed XPS analysis and S.A.H. and M.B. did all cellular experiments supervised by M.C.G. M.C.G. and S.A.H. jointly wrote the manuscript text and all authors reviewed the manuscript.

Additional Information

Supplementary information accompanies this paper at <https://doi.org/10.1038/s41598-018-29674-2>.

Competing Interests: The authors declare no competing interests.

Publisher's note: Springer Nature remains neutral with regard to jurisdictional claims in published maps and institutional affiliations.



Open Access This article is licensed under a Creative Commons Attribution 4.0 International License, which permits use, sharing, adaptation, distribution and reproduction in any medium or format, as long as you give appropriate credit to the original author(s) and the source, provide a link to the Creative Commons license, and indicate if changes were made. The images or other third party material in this article are included in the article's Creative Commons license, unless indicated otherwise in a credit line to the material. If material is not included in the article's Creative Commons license and your intended use is not permitted by statutory regulation or exceeds the permitted use, you will need to obtain permission directly from the copyright holder. To view a copy of this license, visit <http://creativecommons.org/licenses/by/4.0/>.

© The Author(s) 2018